


Vibration Mitigation for a Cryogen-Free Dilution Refrigerator for the AMoRE-Pilot Experiment

C. Lee¹  · H. S. Jo^{1,2} · C. S. Kang¹ ·
G. B. Kim¹ · I. Kim^{1,3,4} · Y. H. Kim^{1,4} ·
H. J. Lee¹ · J. H. So¹

Received: 31 October 2017 / Accepted: 2 June 2018 / Published online: 12 June 2018
© Springer Science+Business Media, LLC, part of Springer Nature 2018

Abstract The Advanced Mo-based Rare process Experiment utilizes a cryogen-free dilution refrigerator to operate its low-temperature detectors. Mechanical vibration originating from its pulse tube refrigerator can affect the detector performance. A mechanical filter system has been installed between the 4K and still plates with eddy current dampers in addition to a spring-loaded damping system previously installed below the mixing chamber plate of the cryostat. The filters significantly mitigated vibrations and improved the detector signals.

Keywords Calorimeters · Double beta decay detectors · Cryocoolers · Cryogenics · Dark matter detectors

1 Introduction

A low-temperature thermometer coupled to a massive absorber is a promising technique for detection of neutrino-less double beta decay [1–3] or weakly interacting massive particles (WIMPs) [4–6] owing to their excellent energy resolution and low

✉ C. Lee
clee21@ibs.re.kr

Y. H. Kim
yhk@ibs.re.kr

¹ Center for Underground Physics, Institute for Basic Science (IBS), Daejeon 34047, Republic of Korea

² Department of Physics, Kyungpook National University, Daegu 41566, Republic of Korea

³ Department of Physics and Astronomy, Seoul National University, Seoul 08826, Republic of Korea

⁴ Korea Research Institute of Standards and Science (KRISS), Daejeon 34113, Republic of Korea

detection threshold. However, such thermometers may also be sensitive to external energy, such as mechanical vibration, entering the detector. Vibration, in particular, may induce friction between the absorber and its support. The released energy is modulated by the thermal circuit and eventually may reach the thermometer, manifesting itself as an unstable baseline. Common sources of vibrations include 1 K-pot [7] or pulse tube refrigerators [8] (PTR) for the precooling of cryostats. Pirro et al. [7,9] presented a set of preliminary vibration isolation stages that were reflected in the design of the CUORE cryostat [10,11].

The AMoRE experiment [12,13] attempts to measure neutrino-less double beta decay of ^{100}Mo . It uses metallic magnetic calorimeters [14] (MMCs) with SQUID readouts to measure phonon and scintillation signals, respectively. For its first run, the vibration from its PTR perturbed the baselines and caused severe deterioration of the phonon and scintillation signals. The deteriorated raw signals also degraded the major performances specifications of the detector, such as energy resolution and particle discrimination via the phonon-to-scintillation ratio [15] or the phonon pulse shape [16]. A preliminary vibration isolation stage called the “mass-spring-damper” (MS) system was devised and installed [17]. Although the results were very successful, they came at the expense of reduced cooling power and experimental space, and the system is not scalable for the future version of the AMoRE experiment.

This article describes further development of vibration isolation methods for the AMoRE-pilot experiment. We present a new mechanical filter, a spring suspended still (SSS) with eddy current dampers (ECDs). The effects of vibration isolation stages can be measured in both the acceleration and the MMC signals.

2 Vibration Isolation

Equation 1 in the notation of our previous work [17], describes the response of a one-dimensional oscillator driven at frequency f with amplitude X_0 and damping ratio η :

$$\frac{x}{X_0} = \frac{1}{\sqrt{\left(1 - \left(\frac{f}{f_0}\right)^2\right)^2 + \left(2\eta\frac{f}{f_0}\right)^2}}. \tag{1}$$

To mitigate vibration, i.e., to decrease x , one desires a minimal f_0 , the natural frequency of the system. To decrease $f_0 = \frac{1}{2\pi}\sqrt{\frac{k}{m}}$ while leaving the mass of the system m fixed, most vibration isolation efforts focus on minimizing the spring constant k .

For practical applications, the effect of gravity should be considered as well. The oscillator drops from its rest position by $\Delta d = \frac{mg}{k}$. The natural frequency can be rewritten using Δd , $f_0 = \frac{1}{2\pi}\sqrt{\frac{g}{\Delta d}}$. This equation is analogous to the pendulum equation, where the extension length Δd replaces the pendulum length l . In fact, a rigid pendulum alone can isolate horizontal vibrations.

The above equation also implies that the available vertical dimension, confining the maximum Δd , limits the lower bound of f_0 . The 1.4 Hz base frequency of PTR vibration is relatively low, and one needs $\Delta d \simeq 25$ cm to produce a natural frequency

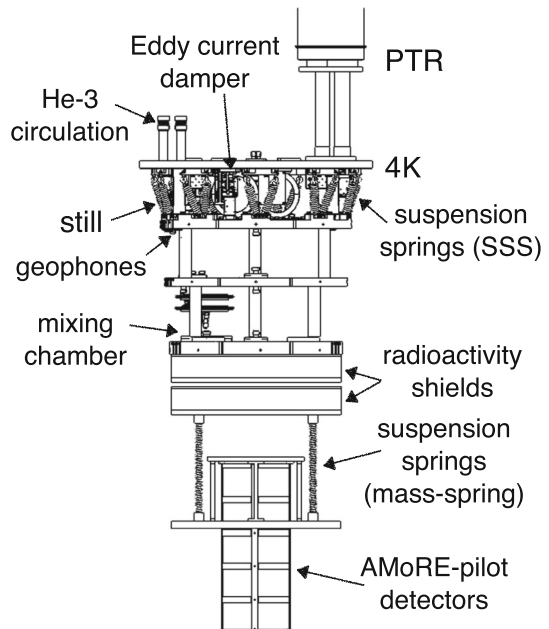
of 1 Hz. This dimension in sample space is not readily achievable in commercially available refrigerators. The isolators discussed below are designed to fit in the mixing chamber and the still assembly.

Although the one-dimensional driven oscillator model is simple and powerful, its effectiveness has limitations in practical applications. First, any real oscillator has at least six degrees of freedom, three linear and three angular, and one of them can be converted into other modes. Second, real springs can store mechanical energy and release it in its internal modes [18]. For the suspension springs, these internal modes are commonly referred to as “surging” frequencies; they are lower for larger wire and coil diameters. Vibrations at multiples of the internal-mode frequencies are transmitted through the isolators. The springs used for the MS and SSS have their first internal modes at approximately 20 and 230 Hz, respectively.

3 Vibration Isolation Stages

Figure 1 shows the vibration isolation stages below the 4K stages of the AMoRE-pilot experiment. For the default Leiden Cryogenics CF-81 1400 dilution refrigerator, the vibration source, PTR, is rigidly bolted on the 4K plate. A radioactivity shield of approximately 250 kg is installed below the mixing chamber. This weight significantly attenuates the vibration at the mixing chamber. The AMoRE-pilot detector module is mechanically decoupled from the PTR via a mass-spring-damper and spring suspended still (SSS).

Fig. 1 Schematic of the AMoRE-pilot detector and its vibration isolation stages



The mass-spring-damper decouples the detectors from the mixing chamber plate of the dilution refrigerator [17]. From its own weight, the detector assembly drops 6 cm from its rest position, and a 2 Hz natural frequency is achieved. Layers of copper tape deliver cooling power to the detectors. Our previous article [17] describes additional technical details of the mass-spring-damper.

The SSS is a new vibration isolation stage introduced for the AMoRE-pilot. It was originally designed by the scanning tunneling microscopy community [19], and a modified version was built for AMoRE by Leiden Spin Imaging B.V. [20]. Here, the still plate is suspended from the 4K plate via a set of stainless-steel springs, and the rigid G11 supporting rods were removed. The rigid LN precooling lines were replaced by flexible lines. The resulting structure has a natural frequency of 3 Hz and provides effective vibration isolation above 10 Hz.

Three eddy current dampers (ECDs) provide damping ($\eta > 0$) and suppress resonances at the lower harmonics of 1.4 Hz [19]. Each ECD consists of two parallel arrays of neodymium permanent magnets and a copper fin in the middle. Vertical motion of the fin relative to the magnets induces resistive force proportional to the velocity of the motion. The gap between the magnet arrays can be adjusted for critical damping ($\eta = 1$). The strength of eddy current and resulting damping force increase at lower temperatures as the resistivity of the copper fin decreases. Stray magnetic fields varying over time can induce unwanted noise in SQUIDs. The permanent magnets form a Halbach array [21, 22] to minimize external stray fields. The magnet arrays are attached to the still flange to reduce its motion relative to the SQUIDs at the mixing chamber.

Compared to the mass-spring-damper, an SSS with ESDs has a few advantages. It does not require extra experimental space. Little cooling power is lost because the ^3He circulation of the dilution unit is left untouched. These advantages make an SSS easy to scale up for a later version of the AMoRE experiment. For the AMoRE-pilot, both the mass-spring-damper and the SSS are used for maximum vibration isolation.

4 Isolation Results

The effect of the SSS was measured at the still flange using Geospace GS-11D geophones. This method is sensitive above 4.5 Hz, the natural frequency of the geophones, and below 500 Hz where the signals diminish below the sensitivity of the geophones. The measurements were made at room temperature and at 4K, where the cryostat operates and the ECDs are most effective. For all spectral density calculations, we averaged two-seconds samples using a Hanning window.

Figure 2 shows the results of the geophone measurements converted to accelerations. Vibrations above 10 Hz are suppressed in both the vertical and horizontal directions. In the *acoustic frequency range*, from 40 Hz to 500 Hz, the average vertical acceleration dropped from 9.1×10^{-5} to $3.4 \times 10^{-6} \text{ m/s}^2/\sqrt{\text{Hz}}$. For the horizontal data, measurements are presented at room temperature instead of at 4K because the geophone malfunctioned during the low-temperature measurement. The room temperature data still show improvements. The horizontal peak at 7 Hz appears to be amplified by the SSS, yet this resonance will be suppressed at 4 K. In the measured

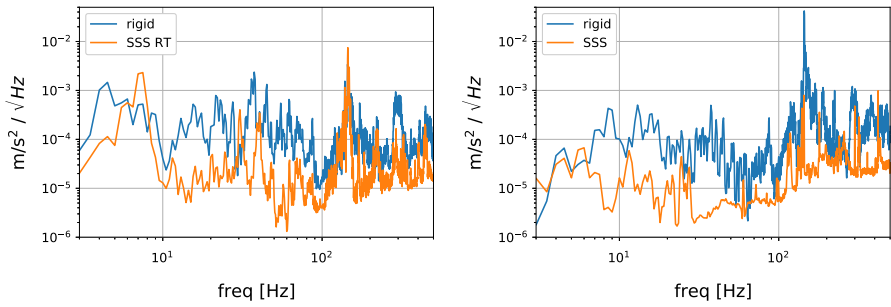


Fig. 2 Acceleration spectrum with PTR on before and after SSS, measured by geophones at the still in the horizontal (*left*, 300 K) and vertical (*right*, 4 K) directions (Color figure online)

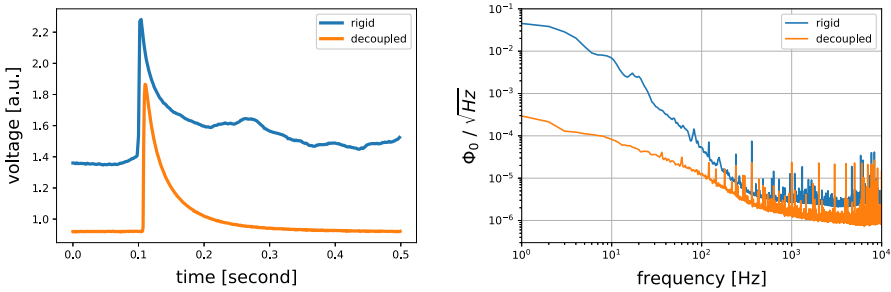


Fig. 3 Crystal 4 signal and noise before (rigid) and after (MS + SSS) vibration isolation. *Left* shows pulses from 2614.5 keV gamma from ²⁰⁸Tl decay overlaid. *Right* compares the baseline noise spectra from the same channel (Color figure online)

Table 1 Comparison of the detector baseline rms integrated from DC to 10 kHz before and after vibration isolation

Channel	2 phonon	3 phonon	4 phonon	2 photon	3 photon	4 photon
Before isolation ($10^{-3} \times \Phi_0$)	108	558	75.6	83.7	48.8	153
After isolation ($10^{-3} \times \Phi_0$)	0.77	0.42	0.60	0.72	4.8	1.6

spectra, several peaks appeared near 145 Hz. We interpret them as mechanical transmission through the liquid nitrogen prerecording lines or the still assembly.

The quality of the heat signal from the MMCs improved significantly as shown in the left illustration of Fig. 3. The noise spectrum of the same channel is shown on the right. Different vibration levels are compared quantitatively by their integrated root-mean-square (rms) power, such that $I = \sqrt{\int_{f_0}^{f_1} D(f)^2 df}$, where $D(f)$ is the sensor signal spectrum. The rms-integrated baselines are compared in Table 1. The baseline improved significantly in all cases.

Light signals improved considerably as well, and example noise spectra are shown in Fig. 4. The rms baseline was reduced by a factor of 850 in this channel. This reduction, however, includes contributions other than the vibration isolation stages, such as modified clamps of the light absorber and better control of the electrical noise

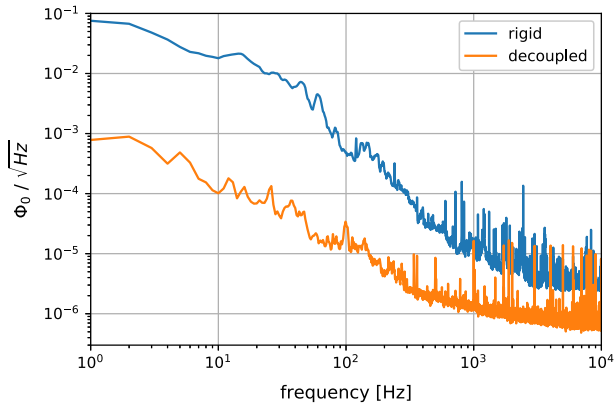


Fig. 4 Crystal 4 photon baseline noise spectrum before (rigid) and after (MS + SSS) vibration isolation (Color figure online)

above 1000 Hz. Further physical interpretation of the noise and signal quality can be found in [23].

5 Conclusions

The mechanical filters effectively mitigated the vibration and improved the heat and light signals of the AMoRE-Pilot experiment. The SSS reduced the acceleration almost by an order in the vertical direction in the 40 to 500 Hz frequency range. For the MMC signals, the rms noise voltage was reduced more than an order of magnitude between DC to 10 kHz. For the best channel, the energy resolution at 2614.5 keV improved to 8.7 keV FWHM, comparable to the data measured in a *wet* dilution refrigerator [24, 25]. The particle discrimination power for alpha against β or γ events has been improved from their pulse shapes and phonon/scintillation ratio [23].

Acknowledgements This work was supported by IBS-R016-G1.

References

1. E. Fiorini, T.O. Niinikoski, Nucl. Inst. Methods A **224**, 83 (1984). [https://doi.org/10.1016/0167-5087\(84\)90449-6](https://doi.org/10.1016/0167-5087(84)90449-6)
2. S.M. Bilenky, Phys. Part. Nuclei **41**, 690 (2010). <https://doi.org/10.1134/S1063779610050035>
3. S.R. Elliott, P. Vogel, Annu. Rev. Nucl. Part. Sci. **52**, 115–151 (2002). <https://doi.org/10.1146/annurev.nucl.52.050102.090641>
4. R. Agnese et al., Phys. Rev. Lett. **116**, 071301 (2016). <https://doi.org/10.1103/PhysRevLett.116.071301>
5. E. Armengaud et al., J. Cosmol. Astropart. Phys. **2016**, 019 (2016). <https://doi.org/10.1088/1475-7516/2016/05/019>
6. G. Angloher et al., Eur. Phys. J. C **76**, 25 (2016). <https://doi.org/10.1140/epjc/s10052-016-3877-3>
7. S. Pirro et al., Nucl. Instrum. Methods A **444**, 331–335 (2000). [https://doi.org/10.1016/S0168-9002\(99\)01376-5](https://doi.org/10.1016/S0168-9002(99)01376-5)
8. K. Uhlig, Cryogenics **42**, 73–77 (2002). [https://doi.org/10.1016/s0011-2275\(02\)00002-4](https://doi.org/10.1016/s0011-2275(02)00002-4)

9. S. Pirro, Nucl. Instrum. Methods A **559**, 672–674 (2006). <https://doi.org/10.1016/j.nima.2005.12.197>
10. C. Ligi et al., J. Low Temp. Phys. **184**, 590–596 (2015). <https://doi.org/10.1007/s10909-015-1389-4>
11. C. Bucci, J. Low Temp. Phys. This special issue (2018)
12. V. Alenkov et al. (2015). [arXiv:1512.05957v1](https://arxiv.org/abs/1512.05957v1)
13. C.S. Kang et al., Supercond. Sci. Technol. **30**, 8 (2017)
14. C. Enss et al., J. Low Temp. Phys. **121**, 137 (2000). <https://doi.org/10.1023/A:1004863823166>
15. G.B. Kim et al., IEEE Trans. Nucl. Sci. **63**, 539–542 (2016). <https://doi.org/10.1109/TNS.2015.2493529>
16. G.B. Kim et al., Adv. High Energy Phys. **2015**, 817530 (2015). <https://doi.org/10.1155/2015/817530>
17. C. Lee et al., J. Inst. **12**, C02057 (2017). <https://doi.org/10.1088/1748-0221/12/02/C02057>
18. J. Winterflood, D.G. Blair, B. Slagmolen, Phys. Lett. A **300**, 122130 (2002)
19. A.M.J. den Haan et al., Rev. Sci. Instrum. **85**, 035112 (2014). <https://doi.org/10.1063/1.4868684>
20. Leiden Spin Imaging B.V. www.leidenspinimaging.com. Accessed 8 June 2018
21. K. Halbach, Nucl. Instrum. Methods **169**, 1 (1980). [https://doi.org/10.1016/0029-554X\(80\)90094-4](https://doi.org/10.1016/0029-554X(80)90094-4)
22. J. Mallinson, IEEE Trans. Magn. **9**, 678–682 (1973). <https://doi.org/10.1109/TMAG.1973.1067714>
23. H.S. Jo et al., J. Low Temp. Phys. (2018). <https://doi.org/10.1007/s10909-018-1925-0>
24. G.B. Kim et al., Astropart. Phys. **91**, 105112 (2017). <https://doi.org/10.1016/j.astropartphys.2017.02.009>
25. I. Kim et al., Supercond. Sci. Technol. **30**, 094005 (2017)